Remote Sensing of Environment 155 (2014) 210–221

Contents lists available at ScienceDirect

Remote Sensing of Environment

journal homepage: www.elsevier.com/locate/rse

Evaluation of the SMAP brightness temperature downscaling algorithm using active–passive microwave observations

Xiaoling Wu [a,*], Jeffrey P. Walker [a], Narendra N. Das [b], Rocco Panciera [c], Christoph Rüdiger [a]

[a] Department of Civil Engineering, Monash University, 3800, Australia
[b] Jet Propulsion Laboratory (NASA), California Institute of Technology, CA 91109, USA
[c] Cooperative Research Centre for Spatial Information, The University of Melbourne, 3053, Australia

ARTICLE INFO

Article history:
Received 22 October 2013
Received in revised form 15 August 2014
Accepted 15 August 2014
Available online 20 September 2014

Keywords:
Downscaling
Brightness temperature
Backscatter
Active–passive
SMAP
SMAPEx

ABSTRACT

The baseline radiometer brightness temperature (*Tb*) downscaling algorithm for NASA's Soil Moisture Active Passive (SMAP) mission, scheduled for launch in January 2015, is tested using an airborne simulation of the SMAP data stream. The algorithm synergistically uses 3 km Synthetic Aperture Radar (SAR) backscatter (σ) to downscale a 36 km radiometer *Tb* to 9 km. While the algorithm has already been tested using experimental datasets from field campaigns in the USA, it is imperative that it is tested for a comprehensive range of land surface conditions (i.e. in different hydro-climatic regions) before global application. Consequently, this study evaluates the algorithm using data collected from the Soil Moisture Active Passive Experiments (SMAPEx) in south-eastern Australia, that closely simulate the SMAP data stream for a single SMAP radiometer pixel over a 3-week interval, with repeat coverage every 2–3 days. The results suggest that the average root-mean-square error (RMSE) in downscaled *Tb* is 3.1 K and 2.6 K for *h*- and *v*-polarizations respectively, when downscaled to 9 km resolution. This increases to 8.2 K and 6.6 K when applied at 1 km resolution. Downscaling over the relatively homogeneous grassland areas resulted in 2 K lower RMSE than for the heterogeneous cropping area. Overall, the downscaling error was around 2.4 K when applied at 9 km resolution for five of the nine days, which meets the 2.4 K error target of the SMAP mission.

1. Introduction

Soil moisture is of great importance to global water cycle monitoring and prediction, especially in agriculture, hydrology and meteorology (Seneviratne et al., 2010; Wagner et al., 2003). With the development of remote sensing technology (Jackson, Hsu, & O'Neill, 2002; Wagner et al., 2007), global mapping of soil moisture from satellites is becoming a viable alternative to traditional monitoring of soil moisture by in situ networks of stations (Hain, Crow, Mecikalski, Anderson, & Holmes, 2011). Consequently, methods are being developed to make use of this emerging soil moisture information to constrain numerical model prediction of soil moisture, and hence improve the forecasting of weather and floods (Albergel et al., 2010; Draper, Mahfouf, & Walker, 2011; Houser, De Lannoy, & Walker, 2012; Reichle, Walker, Koster, & Houser, 2002), leading to significant societal benefits.

Over the past decade, passive microwave remote sensing has emerged as the most promising approach for soil moisture mapping, due to its stronger and more direct connection between the observed brightness temperature (*Tb*) and the near surface soil moisture (top 5 cm), than with active microwave sensing (radar backscatter) or thermal data (Kerr, 2007). The best results were found at low frequency (~1.4 GHz), due to the reduced effects by the atmosphere, surface roughness, vegetation attenuation, and increased observation depth.

The Soil Moisture and Ocean Salinity (SMOS) mission (Kerr et al., 2001) is the first satellite mission dedicated to soil moisture measurement using L-band passive microwave observations, launched by the European Space Agency in 2009. Despite its high sensitivity to near-surface soil moisture, radiometer technology suffers from having a relatively low spatial resolution of approximately 40 km, due to limitations on the maximum antenna size that can be operated in space. Conversely, active microwave observations, which are more difficult to be interpreted for soil moisture content due to the confounding effects of vegetation and surface roughness, have a much finer spatial resolution (<3 km). Therefore, NASA is developing the Soil Moisture Active Passive (SMAP) mission (Entekhabi et al., 2010) scheduled for launch in January 2015 that will take advantage of the synergy between active and passive observations. Accordingly, Das, Entekhabi, and Njoku (2011) have developed a baseline algorithm to overcome the individual limitations of satellite-based L-band radiometer and radar observations.

This baseline algorithm downscales the coarse scale brightness temperatures using the finer resolution radar backscatter cross-sections. The final soil moisture product is then retrieved from the downscaled

* Corresponding author at: Department of Civil Engineering, Room 156/Building 60, Clayton Campus, Monash University, 3800 VIC, Australia. Tel.: +61 3 9905 4957.
E-mail address: xiaoling.wu@monash.edu (X. Wu).

http://dx.doi.org/10.1016/j.rse.2014.08.021
0034-4257/

brightness temperature at 9 km spatial resolution, which is deemed suitable for hydro-meteorological applications such as flood prediction and agricultural activities (Albertson & Parlange, 1999; Weaver & Avissar, 2001). The algorithm has been tested with airborne field campaign data collected by the Passive and Active L-band System (PALS) instrument over various regions of the Continental United States (Das et al., 2011, 2014). However, more extensive testing of the algorithm over different land covers and hydro-climatic regimes is imperative before application to the global SMAP data stream. The target accuracy of this brightness temperature downscaling algorithm is 2.4 K as explicitly stated in the SMAP Algorithm Theoretical Basis Document (ATBD, Entekhabi, Das, Njoku, Johnson, & Shi, 2012).

Other downscaling approaches have been studied using synthetic active and passive observations, such as the Bayesian merging algorithm (Zhan, Houser, Walker, & Crow, 2006), which uses an inherently different strategy, resulting in a downscaled soil moisture product directly through the synergy of the active and passive data in a Bayesian framework. However, such a technique has only been tested in an Observation System Simulation Experiment (OSSE) framework not with real data. A further candidate downscaling approach is based on the change detection method, using the assumption of an approximately linear dependence of radar backscatter and brightness temperature change on soil moisture change (Narayan, Lakshmi, & Jackson, 2006; Piles, Entekhabi, & Camps, 2009). However, this downscaling algorithm has limitations because of its operational implementation, and is not well-tested using field campaign data.

In this study, the baseline brightness temperature downscaling method for the SMAP mission (Das et al., 2014), which is based on the assumption of a near-linear relationship between radar backscatter (σ) and radiometer brightness temperature (Tb), is tested using airborne passive and active microwave observations collected over a semi-arid landscape during the Soil Moisture Active Passive Experiments (SMAPEx) conducted in Australia in 2010–2011, allowing assessment of the robustness of this baseline downscaling algorithm over different land conditions. The linear regression parameters are estimated using SMAP-type passive and active microwave data at 36 km resolution. These parameters are then applied in the algorithm using aggregated radar data at 3 km to derive downscaled passive microwave observations at 9 km resolution, with the objective to evaluate the accuracy of the brightness temperature downscaling method. Although the ultimate objective of the SMAP mission is to produce a downscaled soil moisture product, this can only be achieved once the assumption that the baseline brightness temperature downscaling procedure is sufficiently accurate. Subsequent to this, the standard and well-accepted passive microwave soil moisture retrieval algorithms are applied. Therefore, the purpose of this paper is to challenge the baseline brightness temperature downscaling approach as proposed in the SMAP ATBD (Das et al., 2014; Entekhabi et al., 2012) and to test its robustness in terms of the downscaled brightness temperature values, according to the requirements set out in ATBD (Entekhabi et al., 2012). Testing of the final soil moisture retrieval accuracy following the downscaling of the brightness temperature is outside the scope of this study.

2. Data set

The Soil Moisture Active Passive Experiments (Panciera et al., 2014) comprised a series of three campaigns undertaken over a one-year time frame (winter July 5–10, 2010; summer December 4–8, 2010; and spring September 5–23, 2011), and were specifically designed to contribute to the development of radar and radiometer soil moisture retrieval algorithms for the SMAP mission. The SMAPEx study area, with a size of approximately 38 km × 36 km, is situated within the Murrumbidgee River catchment (34.67°S, 35.01°S, 145.97°E, 146.36°E) as shown in Fig. 1. This site was chosen for testing the SMAP downscaling algorithm performance due to its flat topography, high density of soil moisture monitoring stations, and spatial variability in soil, vegetation and land use.

The SMAPEx area is characterized as semi-arid with a relatively flat topography, comprising of approximately 30% cropping area. The soil types are predominantly clays, red brown earths, and sand over clay, thus allowing an investigation of the downscaling algorithm under unique geophysical and meteorological conditions that are so far not tested for the downscaling algorithm. As shown in Fig. 1, the western part of the SMAPEx site is dominated by cropping areas, while the eastern half consists mostly of grassland areas, including a large water body in the north-eastern quarter (approximately 500 m × 5 km in size). Some woodlands along the south-to-north flowing Yanco River, as well as some small forest areas in the far East of the SMAPEx area, are also present. This study site represents the heterogeneous land cover conditions that are typical of many landscapes, and thus required to evaluate the robustness of the SMAP active–passive baseline downscaling algorithm performance.

The SMAPEx airborne instruments allowed the acquisition of concurrent active and passive microwave remote sensing measurements at 1.26 GHz and 1.41 GHz (L-band) frequencies respectively, being the same as the future SMAP sensors. Those data were collected by covering an area the size of a SMAP radiometer footprint (approximately 36 km × 38 km for the EASE grid at 35°S latitude) over a landscape typical of south-eastern Australia, using a research aircraft. The SMAPex airborne instrument suite consists of the Polarimetric L-band Multibeam Radiometer (PLMR) and the Polarimetric L-band Imaging Synthetic Aperture Radar (PLIS), which when used together on the same aircraft can provide a SMAP-like data stream for developing and testing of the algorithms applicable to the SMAP mission viewing configuration. The SMAPEx flights also mimicked a time series of SMAP-like observations with a 2–3 day revisit time. A complete description of the experiment design can be found in Panciera et al. (2014).

In order to closely replicate the prototype SMAP data stream for development and testing of the downscaling techniques, data collected during the SMAPEx field campaigns were processed in terms of resolution aggregation (36 km for passive and 3 km for active) and incidence-angle normalization (to 40° reference angle), to be in line with the spatial resolutions of SMAP (Wu, Walker, Rüdiger, Panciera, & Gray, in press). The accuracy of the simulated SMAP data stream used in this study has been determined as comparable to the error budget of the SMAP data stream, which is approximately 1.0 dB for backscatter at 3 km resolution and 1.3 K for brightness temperature at 36 km resolution (Wu et al., in press). The original resolutions of the data sets are 1 km for the PLMR brightness temperatures and 10–30 m for the PLIS backscatter. Since they have been upscaled to 36 km and 3 km respectively for the purpose of application, the PLIS data were also aggregated to 1 km and 9 km to evaluate the performance of the SMAP downscaling algorithm at different spatial resolutions, since the native resolution of the SMAP radar is actually 1 km. Moreover, the reference Tb data used for evaluation of the downscaling results come from the original 1 km PLMR, and were therefore aggregated to resolutions of 3 km and 9 km for use as reference at a range of scales.

The radiometer and radar data used to test this baseline downscaling algorithm were from the third SMAPEx campaign (SMAPEx-3, September 5–23, 2011), which was conducted during the spring vegetation growing season. This campaign was used since it comprised nine regional flights over a 3-week time period with the 2–3 day revisit time of SMAP. A sample of the simulated SMAP data stream used in this study is shown in Fig. 2.

3. Methodology

The baseline downscaling algorithm (Das et al., 2014) to be implemented for the SMAP mission aims to merge coarse resolution L-band passive microwave brightness temperature (Tb, in Kelvin) with fine resolution L-band active microwave backscatter coefficient (σ, in decibel)

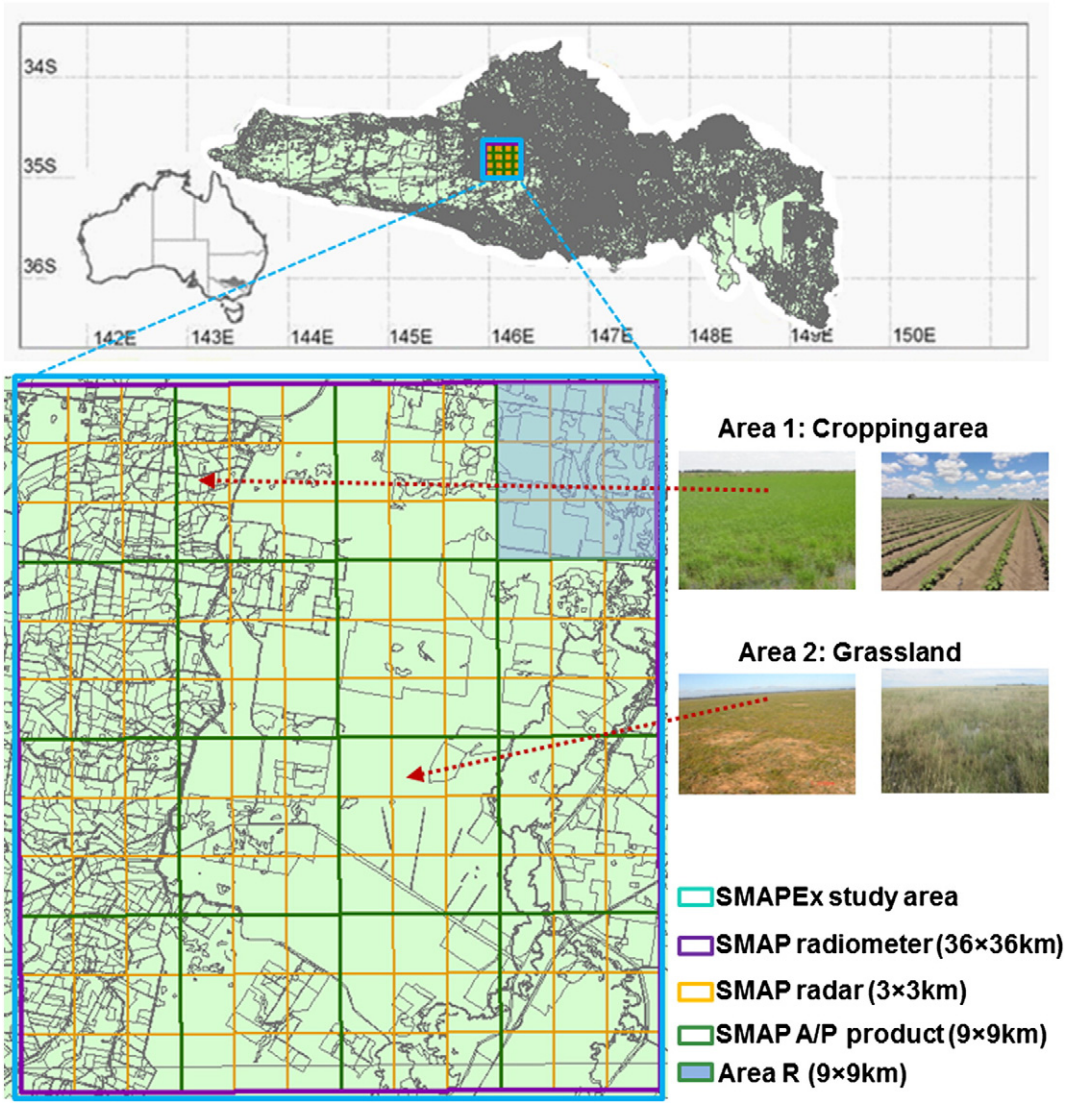

Fig. 1. Overview of the SMAPEx site showing the SMAP pixel sized study site, and the SMAP grid on which the 36 km resolution radiometer data, 3 km resolution radar data and 9 km resolution active–passive downscaled product will be provided, together with area *R* in the north-eastern corner where the rainfall events happened during the third SMAPEx field campaign.

based on the main assumption of a near-linear relationship between them when observed at the same time, scale, and incidence angle. The algorithm is briefly described in the following paragraphs, while a complete description is available in Das et al. (2014).

In the following the naming convention of '*C*' (coarse), and '*F*' (fine) represents the *Tb* and/or σ at 36 km and 3 km, respectively. Implementation of this method requires a background *Tb* at *C* resolution, with the variation of *Tb* imposed by the distribution of fine scale σ within *C* modulated by $\beta(C)$ using the linear regression between *Tb* and σ at *C* resolution according to:

$$Tb_p\left(F_j\right) = Tb_p(C) + \beta(C) \times \left\{\left[\sigma_{pp}\left(F_j\right) - \sigma_{pp}(C)\right] + \Gamma \times \left[\sigma_{pq}(C) - \sigma_{pq}\left(F_j\right)\right]\right\}. \quad (1)$$

where *p* indicates the polarization, including *h*- and *v*-pol; and *pp* means co-polarization of radar observations σ, including *hh* or *vv*-pol. Correlations between four different combinations of Tb_p and σ_{pp} have been analyzed and will be presented in this paper. $Tb_p(F_j)$ is the brightness temperature value of a particular pixel "*j*" of resolution *F*, and $\sigma_{pp}(F_j)$ is the corresponding radar backscatter value of pixel "*j*". In this study the value for $\sigma_{pp}(C)$ (in the unit of dB) was obtained by aggregating 10 m resolution PLIS data (in power units) within the coarse footprint *C*, with $Tb_p(C)$ aggregated from 1 km resolution PLMR observations (in Kelvin). Consequently, $\beta(C)$, which depends on vegetation cover and type as well as surface roughness, is assumed to be time-invariant and homogenous over the entire 36 km pixel and that it can be obtained through the time-series of $Tb_p(C)$ and $\sigma_{pp}(C)$. Since the radar also provides high-resolution cross-polarization (*hv*-pol) backscatter measurements at resolution *F*, which is mainly sensitive to vegetation and surface roughness, the sub-grid heterogeneity of vegetation/surface characteristics within resolution *C* can be captured as $[\sigma_{pq}(C) - \sigma_{pq}(F_j)]$ by the radar, where *pq* represents *hv*-pol. This heterogeneity indicator is then converted to variations in co-polarization *pp* backscatter by multiplying a sensitivity parameter Γ for each particular grid cell *C* and season defined as $\Gamma = [\delta\sigma_{pp}(F_j) / \delta\sigma_{pq}(F_j)]_C$. In other words, the

Fig. 2. Example of the simulated SMAP prototype data from PLMR and PLIS observations across 9 days of SMAPEx-3 experiment (D1 to D9), with incidence angle normalized to 40°: (a) backscatter (σ) at *vv*-polarization and at 3 km resolution aggregated from PLIS; (b) brightness temperature (*Tb*) at *v*-polarization and at 36 km resolution aggregated from PLMR; (c) *Tb* at *v*-polarization and at 3 km resolution aggregated from PLMR; (d) *Tb* at *v*-polarization and at 9 km resolution aggregated from PLMR.

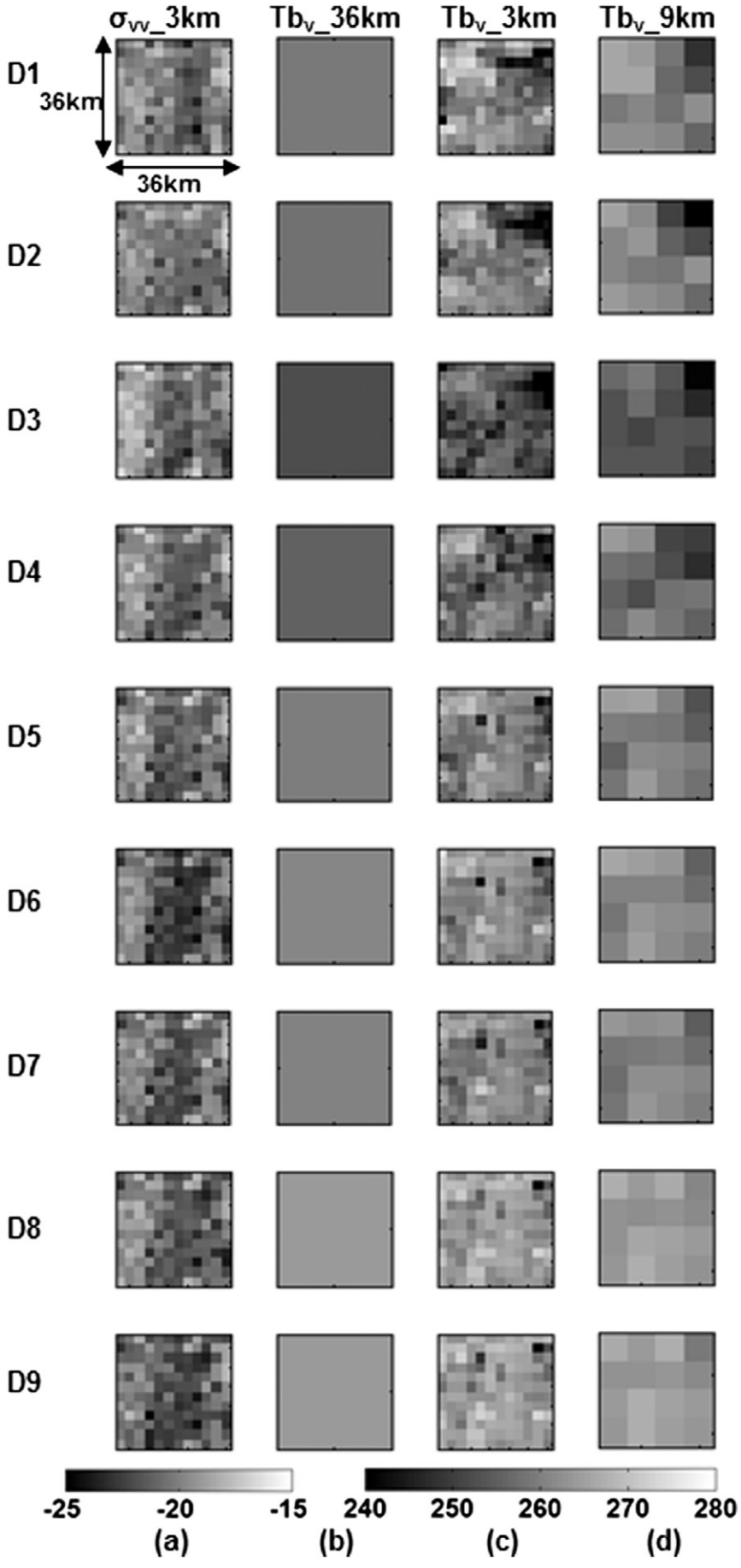
σvv_3km
Tbv_36km
Tbv_3km
Tbv_9km
D1
36km
36km
D2
D3
D4
D5
D6
D7
D8
D9
-25
-20
-15
240
250
260
270
280
(a)
(b)
(c)
(d)

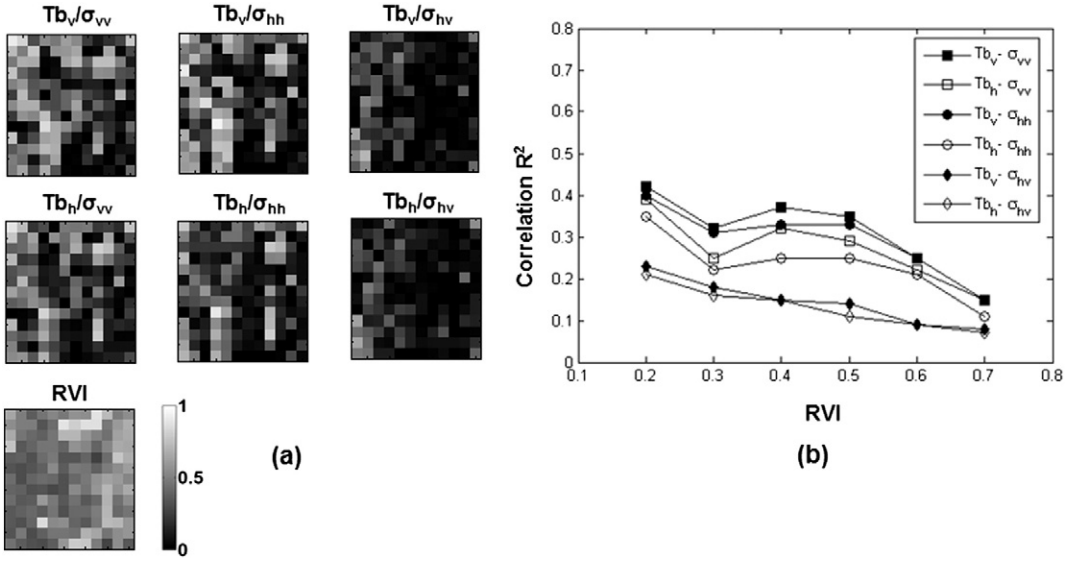

Fig. 3. (a) Correlation between brightness temperature (*Tb*) and backscatter (σ) at different polarizations as shown, and spatial distribution of average Radar Vegetation Index (RVI) across the 9 days (both correlation coefficient and RVI are displayed on a scale from 0 to 1) at 3 km spatial resolution; (b) plot of these correlation coefficients between *Tb* and σ at different polarizations according to RVI.

term $\Gamma \times [\sigma_{pq}(C) - \sigma_{pq}(F_j)]$ can be described as the projection of the cross-polarization sub-grid heterogeneity onto the co-polarization space, thus converting the information of vegetation and surface characteristics to the variation of co-polarization backscatter. This term is converted to brightness temperature through multiplication by $\beta(C)$ in Eq. (1).

Using Eq. (1) in this study, the 36 km resolution *Tb* is downscaled to 3 km resolution. The *Tb* at the intermediate resolution, i.e. 9 km, can be obtained by two methods: i) directly upscaling the 3 km downscaled *Tb* to 9 km through linear aggregation; or ii) first averaging the backscatter data (in power unit) from 3 km to 9 km, and subsequently using it in place of the fine resolution backscatter data in Eq. (1). Both methods are assessed in this paper. Moreover, due to the high resolution backscatter provided by the SMAPEx airborne instruments, the 36 km resolution *Tb* can be downscaled to 1 km resolution using 1 km resolution σ, thus assessing the skill of this downscaling algorithm at three different scales: 1 km, 3 km and 9 km.

The downscaled *Tb* at fine resolution is heavily dependent on the quality of the overall radiometer data at coarse scale, the relative backscatter difference within the coarse grid, and the relationship with *Tb* as represented by the regression slope that is added to the background value. The performance of the downscaling algorithm at different resolutions is evaluated by comparing the downscaled *Tb* with the PLMR *Tb* data at 1 km, 3 km and 9 km resolutions (aggregated from its original 1 km resolution), respectively, in order to assess the merit of this downscaling method in preparation for SMAP.

4. Results

4.1. Robustness of the linear active–passive relationship

The robustness of the linear relationship between *Tb* and σ is tested in this section for the six possible polarization combinations (i.e. Tb_h and σ_{hh}, Tb_v and σ_{hh}, Tb_h and σ_{vv}, Tb_v and σ_{vv}, Tb_h and σ_{hv}, Tb_v and σ_{hv}), aiming to determine the best combination for estimating the parameter β. Consequently, the brightness temperature and backscatter observations from PLMR and PLIS were spatially aggregated to 3 km resolution, resulting in a total of 144 pixels within the study area, presenting different levels of vegetation heterogeneity. Examples of those data are shown in Fig. 2(a) and (c).

The correlation coefficient R^2, used to quantify the correlation between *Tb* and σ for each 3 km pixel, was calculated using the entire time series of *Tb* and σ of each individual pixel. Results for the different polarization combinations are shown in Fig. 3. Out of those, σ at *vv*-polarization showed the best correlation with *Tb* at both *h*- and *v*-polarizations; these results are in good agreement with those presented in Das et al. (2011). Therefore, the relationships of σ_{vv} and Tb_v were used to estimate β at *v*-pol, while σ_{vv} and Tb_h were used to estimate β at *h*-pol, thus retrieving the downscaled *Tb* at *h*- and *v*-pol, respectively.

The influence of vegetation conditions on the correlation between *Tb* and σ was also investigated. The Radar Vegetation Index (RVI) was introduced as an indicator of the compound vegetation conditions (including vegetation water content, vegetation biomass), which can be obtained directly from the radar observations using the different polarizations by

$$\mathrm{RVI} = 8 \times \sigma_{hv}/(\sigma_{vv} + \sigma_{hh} + 2 \times \sigma_{hv}), \quad (2)$$

where the radar backscatter values are in units of power (Kim & van Zyl, 2009). Fig. 3 shows the average RVI values in each 3 km pixel calculated from the 9 days of radar observations aggregated to 3 km, in order to characterize the vegetation conditions. This was done assuming that vegetation conditions (and thus their associated RVI values) did not change significantly across the 3-week period. For this experiment, the standard deviation (in time) of the RVI was found to be less than 0.1 across the entire study area.

While the R^2 between *Tb* and σ was generally larger in the western two thirds than in the east of the SMAPEx area, the values of RVI were smaller in the west than in the east. Although it was expected that the highest correlation would be for low vegetation areas, the reason for the higher RVI in the east is due to some small forests in the area and trees along the Yanco River (see Fig. 3). This indicates that the downscaling algorithm performance will be poorer in areas with denser vegetation.

The sensitivity of *Tb* to changes in σ was analyzed using the slope of the linear regression (parameter β) as a measure of quality. The relationship between β and RVI is displayed in Figs. 4 and 5, with Fig. 4 showing the relationship between Tb_v and σ_{vv} anomalies under different vegetation conditions (i.e. different RVIs), and the sensitivity parameter β estimated from observations of Tb_v and σ_{vv} within the entire

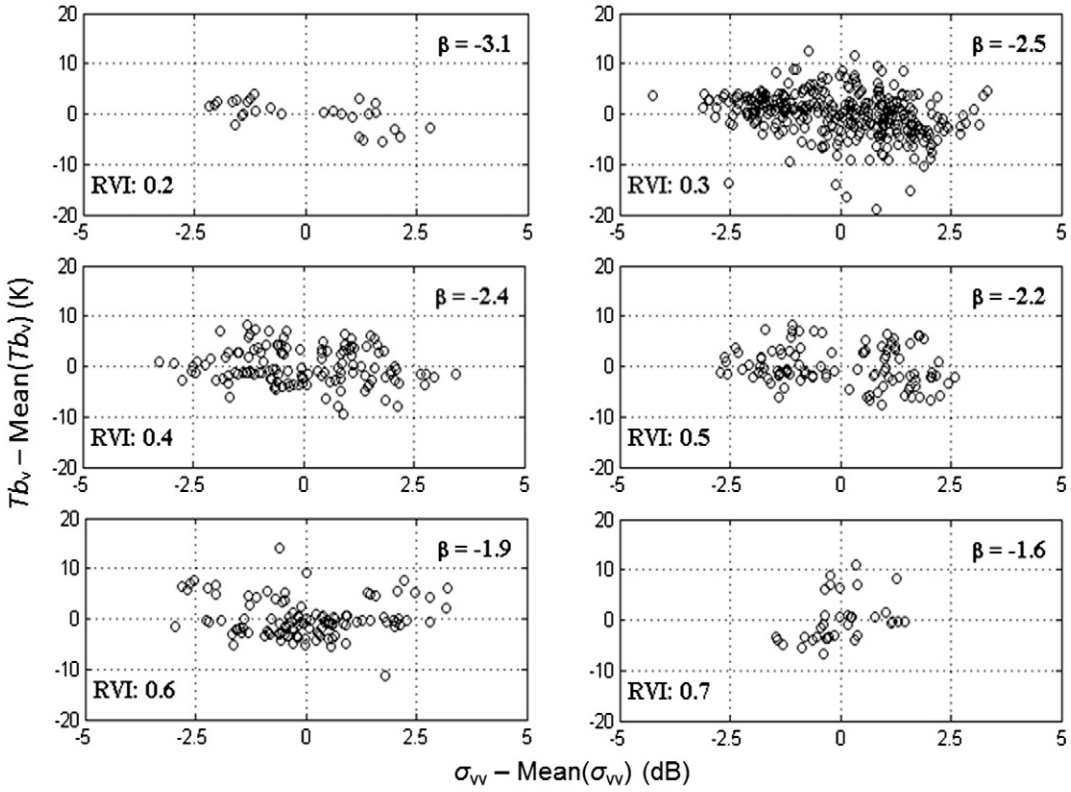

Fig. 4. Relationship between brightness temperature at *v*-polarization (Tb_v) and backscatter anomalies at *vv*-polarization (σ_{vv}) at 3 km resolution, for different vegetation characteristics according to the Radar Vegetation Index (RVI) calculated from 3 km radar observations.

study area. Both RVI and β were aggregated to 3 km resolution. These scatter plots show that: 1) Tb_v and σ_{vv} have a near-linear relationship; 2) the magnitude of β reduces as vegetation density increases, indicating that the sensitivity of brightness temperature to backscatter decreases, thus showing the dependence of sensitivity on the vegetation density. Fig. 5 shows the parameter β and its associated standard deviation plotted as a function of the RVI. The standard deviation of β estimation is higher at the RVI extremes, mainly due to the limited counts of Tb and σ pairs for those values. According to the numbers of points in each plot, most of the points are within the range of RVI from 0.3 to 0.6, indicating that vegetation with RVI 0.3–0.6 dominates this study area. Investigation of the relationship between RVI and the accuracy of the downscaling algorithm for a specific area is out of the scope of this study, but will possibly provide a direct method of estimating the downscaling performance globally from SMAP radar observations.

Given that σ_{vv} showed the best correlation with Tb_v, the sensitivity parameter β for performing the downscaling in this study has been estimated based on the combination of Tb_v and σ_{vv}. In this particular downscaling algorithm, β was estimated from Tb and σ data both aggregated to 36 km resolution, in order to align with the resolutions of SMAP. As a result, using the 9-days' time series of aggregated Tb_v and σ_{vv}, β over the entire area has been estimated as approximately −2.2 K/dB, with the average RVI across the whole area being around 0.5, aligning with the correlation between β and RVI as shown in Figs. 4 and 5. The same approach was applied to estimate β using Tb_h and σ_{vv}, for the downscaling of Tb at *h*-pol. In this case, similar trends

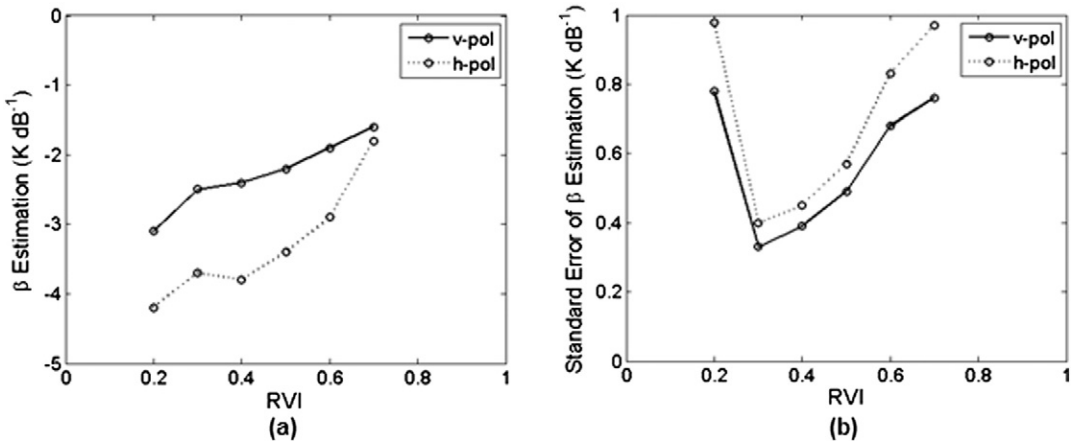

Fig. 5. Dependency of regression parameter β (a) and associated standard deviation (b) of estimation from the Radar Vegetation Index (RVI) at 3 km resolution. The β at *h*- and *v*-polarizations was estimated using backscatter (σ) at *vv*-polarization for brightness temperature (Tb) at *h*- and *v*-polarizations.

for β estimation and its standard error were found with respect to RVI, as shown in Fig. 5. However, the magnitude of β at different RVIs is on average 1.2 K/dB higher than that estimated from Tb_v and σ_{vv}, implying that the sensitivity of Tb_h to σ_{vv} is higher than the sensitivity of Tb_v to σ_{vv}. Regardless of the actual variation of vegetation within the entire area, β was estimated as a single value across the 36 km area as outlined in the SMAP baseline active–passive algorithm. Based on this preliminary analysis of the relationship between RVI and β, it is suggested that a more detailed investigation of the spatial distribution of β within the 36 km area should be undertaken, including an investigation of a potential spatially varying β implementation in the SMAP baseline algorithm.

4.2. Estimation of Γ

The parameter Γ, i.e. the sensitivity of σ_{vv} to σ_{hv}, can be estimated using snapshots of σ_{vv} and σ_{hv} values at each pixel within a certain area. Since radar backscatter σ at *hv*-pol is more related to the vegetation canopy than to the soil, the distribution of σ_{hv} across the entire area can be used to characterize the heterogeneity of vegetation conditions in that area. Therefore, downscaling results can be improved by including the influence of vegetation on the backscatter observation, by converting the σ_{hv} variation within the entire area to σ_{vv} variation, by multiplying with the sensitivity Γ.

In order to obtain an estimate for the parameter Γ, the study area was divided into 16 sub-areas of 9 km by 9 km in size, and the value of Γ was calculated using the snapshots of all σ_{vv}–σ_{hv} pairs at 1 km resolution contained within each of those sub-areas, allowing an analysis of the relationship between estimation of Γ and RVI. Accordingly, the day-to-day variation and average of Γ with respect to RVI are shown in Fig. 6, together with an example of the distribution of Γ at each 9 km sub-area across the entire study area on Day 9 (23rd September, 2011). It is shown that for RVI values ranging from 0.4 to 0.9 the estimation of Γ is similar, on the order of 0.45, while for RVI values less than 0.4, Γ is much higher, indicating that the sensitivity of σ_{vv} to σ_{hv} increases when the vegetation cover reduces. Again, larger standard deviations were found for both extremes due to low counts of pixels.

4.3. Accuracy of downscaling

According to the baseline approach the downscaled brightness temperature at fine resolution are a function of the background *Tb* value plus a variation of *Tb* within the entire area derived from the variation of the backscatter from the mean. In this study, the background *Tb* is taken as the aggregated 36 km *Tb* from PLMR, and the variation of *Tb* at higher resolution is characterized by the variation of σ_{vv} from PLIS observations, aggregated to the downscaling resolution. The influence of vegetation is then deduced using σ_{hv}, due to its strong correlation with vegetation conditions. Consequently, the downscaled *Tb* results were retrieved at resolutions of 1 km, 3 km and 9 km, either from aggregating the 1 km resolution downscaled *Tb* to 3 km and 9 km resolution respectively, or from first aggregating the 1 km resolution radar observations to 3 km and 9 km before using them to disaggregate the 36 km *Tb*. Both methods were applied and showed similar results; results shown in this paper are based on the former method. Prior to applying the downscaling algorithm, the main water body in the far north-eastern section of the area, and some irrigated cropping areas within the western part of the regional area, were removed (these areas collectively represented approximately 1% of the entire study region) to reduce the influence of surface water on the resulting downscaling accuracy.

Based on the estimation of β at *h*- and *v*-polarizations and the day to day matrix of Γ estimates derived in the previous sections, the baseline downscaling algorithm performance was evaluated for each of the nine days of SMAPEx airborne acquisitions. In order to analyze the influence of vegetation characteristics on the resulting downscaled *Tb*, the downscaling algorithm was applied in two scenarios: in scenario "A1", the vegetation heterogeneity across the study area was ignored; in scenario "A2", the vegetation heterogeneity across the study area was taken into account. In other words, A1 was characterized by setting $\Gamma = 0$, while A2

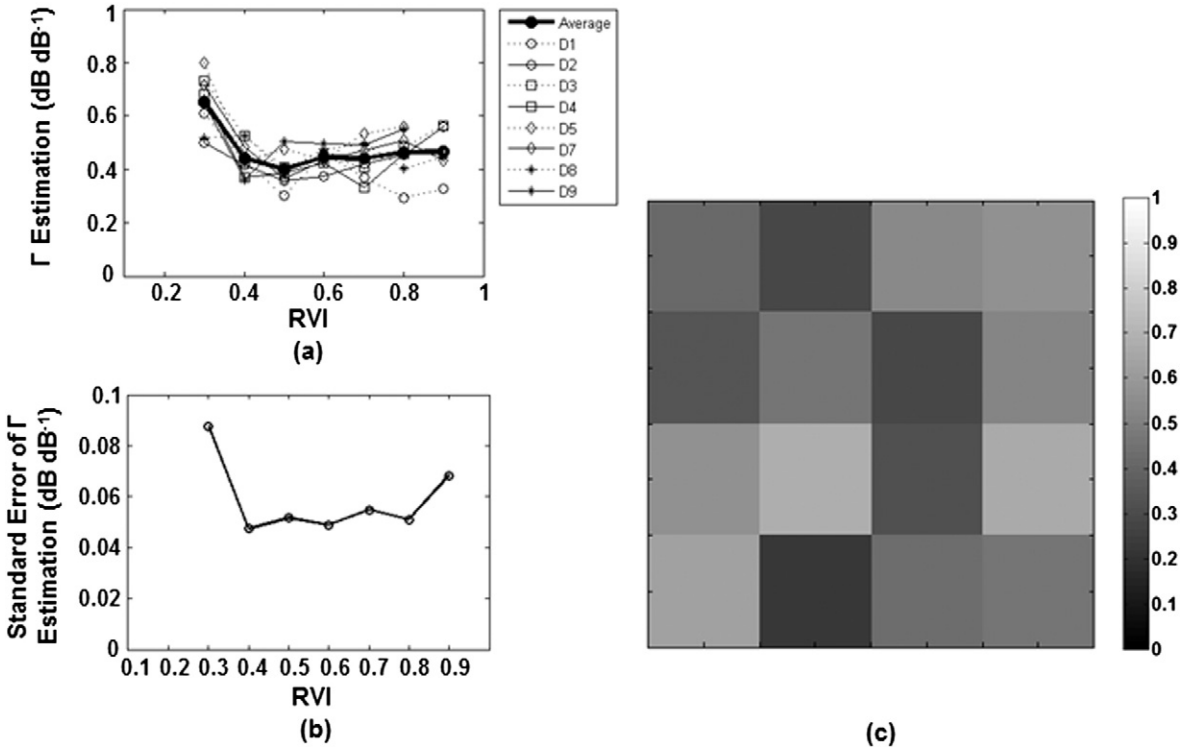

Fig. 6. Estimation of parameter Γ: (a) Γ plotted as a function of the Radar Vegetation Index (RVI) on different days; (b) standard deviation of Γ estimation; and (c) example of Γ distribution over the entire study area on Day 9; each pixel has a size of 9 km × 9 km (low: 0.3; high: 0.6).

Table 1
Accuracy of the SMAP baseline downscaling algorithm. Root mean square error (RMSE) between downscaled brightness temperature (*Tb*) and reference *Tb* is shown for the entire study area across the 9-days (D1 to D9) with respect to polarization and resolution of the final downscaled product; results based on scenario A1 ($\Gamma = 0$) and scenario A2 ($\Gamma \neq 0$) are shown.

Downscaling resolution (km)		D1		D2`		D3		D4		D5		D6		D7		D8		D9		Average	
		h	*v*	*h*	*v*	*h*	*v*	*h*	*v*	*h*	*v*	*h*	*v*	*h*	*v*	*h*	*v*	*h*	*v*	*h*	*v*
1	A1	11.7	9.1	10.4	8.2	10.5	7.9	10.6	8.3	9.1	6.8	9.0	6.7	8.1	6.0	8.4	6.2	8.2	5.8	9.5	7.2
	A2	10.5	8.4	9.5	8.0	9.0	7.1	9.2	8.0	8.1	6.2	8.1	6.1	6.3	5.2	7.0	5.6	6.6	5.1	8.2	6.6
3	A1	9.1	7.0	7.7	6.1	7.6	5.6	7.6	5.9	5.8	4.4	6.2	4.3	5.1	3.6	5.4	3.8	5.2	3.6	6.6	4.9
	A2	8.6	6.7	7.3	6.0	5.6	4.6	6.8	5.5	4.9	4.2	5.2	4.1	4.2	3.3	4.2	3.3	3.3	3.2	5.5	4.5
9	A1	6.0	4.7	4.7	3.9	4.9	3.5	4.9	3.8	3.2	2.5	3.3	2.4	2.5	1.8	3.2	2.2	2.9	1.8	3.9	2.9
	A2	5.8	4.5	4.6	3.7	3.9	3.1	4.0	3.5	2.5	2.4	2.4	2.1	1.5	1.5	2.0	1.7	1.9	1.5	3.1	2.6

used $\Gamma \neq 0$ in Eq. (1). In the following, the results of the downscaling are compared among the two scenarios.

Downscaling results on each day of SMAPEx-3 are shown in Table 1 for different resolutions and polarizations. It is noted from Table 1 that the downscaled results at *v*-polarization had relatively lower RMSE than those at *h*-polarization, likely due to the better correlation between σ_{vv} and Tb_v than between σ_{vv} and Tb_h. Moreover, there is an obvious reduction of RMSE at both polarizations when applied to a larger scale, e.g. from 1 km to 3 km and 9 km respectively, which can be attributed to the reduction of random (white) noise following the aggregation of the backscatter data.

Apart from resolution and polarization, the RMSE was further reduced when taking into account the variation of vegetation across the entire area, confirming that the Γ term in Eq. (1) can be used to compensate the influence of vegetation conditions to some degree, thus yielding a more accurate finer resolution brightness temperature product. Quantitative results are provided in Table 1, showing that the average RMSE of the 9 days at *v*-polarization was lower by 1–2 K than at *h*-polarization, and decreased by approximately 5 K when aggregating from 1 km to 9 km. As before, after considering the influence of vegetation heterogeneity (scenario A2 with $\Gamma \neq 0$), the RMSE of downscaled *Tb* had an improvement of 1.2 K at *h*-polarization and 0.5 K at *v*-polarization over the results based on the assumption of a homogeneous vegetation (scenario A1, $\Gamma = 0$). Moreover, during 5 out of 9 days the RMSE was found to be around 2.4 K at 9 km resolution, which is within the target error of the SMAP mission (2.4 K when the vegetation water content is less than 5 kg/m^2), confirming that the baseline downscaling algorithm has the potential to retrieve medium resolution brightness temperature with an error of around 2.4 K over heterogeneous areas.

In order to confirm that the use of σ_{vv} is more efficient than σ_{hh}, as suggested by the correlation analysis between *Tb* and σ, an additional test was performed using coarse resolution *Tb* and fine resolution σ_{hh} to retrieve *Tb* at scales of 1 km, 3 km and 9 km. The performance levels of the algorithm using σ_{vv} and σ_{hh} are presented in Table 2, showing that the RMSE based on σ_{vv} is around 0.2 to 0.9 K lower than that based on σ_{hh}, confirming the results from Fig. 3 where there was a stronger correlation of σ_{vv} to *Tb* than σ_{hh}.

Examples of downscaled *Tb* maps are shown in Fig. 7 for Day 9 at 1 km, 3 km and 9 km resolutions, alongside the reference data from PLMR, and the pixel-by-pixel *Tb* difference between downscaled and reference values. It is noted that the downscaling errors are generally larger in the western part of the study area than the central section, which is mainly due to the western part being dominated by irrigated and dry-land cropping areas, while the central area is largely covered by grassland. A consequence of the large heterogeneity of the cropping areas was a relatively large RMSE in those areas, as highlighted by the RMSE behavior from west to east of the entire region in Fig. 8. Dependence of RMSE for the 36 strips (each with 1 km width when progressing from west to east and having 36 km length in the north–south direction) covering the SMAPEx study area is displayed in Fig. 8. Overall, the RMSE of the central area, the dominantly grassland area between distances of 18 km and 28 km, is around 2 K lower than elsewhere.

Table 2
Downscaling algorithm performance in terms of root mean square error (RMSE) when using backscatter at *hh*- and *vv*-polarizations, together with the RMSE difference between these two polarizations.

Downscaling resolution (km)	σ_{vv}		σ_{hh}		Difference	
	h	*v*	*h*	*v*	*h*	*v*
1	8.2	6.6	9.1	7.2	−0.9	−0.6
3	5.5	4.5	6.2	5.0	−0.7	−0.5
9	3.1	2.6	3.3	3.3	−0.2	−0.2

As shown in Figs. 3 to 5, β estimation should be lower than −3 K/dB (at *v*-pol) and −4 K/dB (at *h*-pol) in the western area and should be higher than −2 K/dB (at *h*- & *v*-pol) in the eastern area due to the variation in RVI across the entire region. However, since the constant value of β from 36 km *Tb* and σ is used in this study, which is −2.2 K/dB (at *v*-pol) and −3.4 K/dB (at *h*-pol), there is an under-estimation in the west and over-estimation in the east, which is directly related to the magnitude of β variation from the nominal value used and therefore further influencing the accuracy of this downscaling algorithm. Moreover, the RMSE in the east is relatively high, due to the influence from the large areas of woodland along the river which runs approximately south to north in that part, and some other areas of dense forest.

A further evaluation of the skill of this particular downscaling algorithm was through the correlation between downscaled and reference *Tb* at 9 km resolution (Figs. 9 and 10). While these two black dashed lines represent RMSE less than 2.4 K (the SMAP target), the outer two black solid lines represent RMSE less than 4 K (the SMOS target). It is noted from Figs. 9 and 10 that more than 93% of the points from D3 ("D" represents "Day") to D9 are within the SMOS target range, and five of them (from D5 to D9) have more than 90% of points within the SMAP target range, showing that the baseline downscaling algorithm can provide accurate *Tb* at 9 km.

Nonetheless, the results of the first days i.e. D1 to D4 displayed relatively poor performance when compared to the later days. In particular, D1 and D2 contain significant noise levels. One possible reason is attributed to increased heterogeneity in near surface soil moisture due to the heavy rainfall events in the northeastern part of the study area at the beginning of SMAPEx-3 as shown in Figs. 1 and 2(c), subsequently resulting in more heterogeneous radiometer and radar observations. It is shown in Figs. 9 and 10 that D1 to D4 had a higher standard deviation of *Tb* (reference *Tb*) when compared to the other days. Since *Tb* is more sensitive to the immediate soil moisture changes due to the rain in this region, the value of *Tb* drop according to soil moisture increase is more significant than the radar backscatter changes, as the latter is more influenced by the vegetation cover and consequently less sensitive to the soil moisture changes. Consequently, the sensitivity of backscatter to *Tb* change decreases, resulting in an obvious difference in β for the area subjected to rainfall when compared with the other drier areas, which would have dominated the derivation of the β value used. This is underlined by the RMSE in the north-eastern part (area *R*) of the study area being around 3 K higher than throughout the remaining area (at 3 km resolution), impacting the overall large RMSE for that day, as shown in Fig. 11. In addition, the average RVI of area *R* is ~0.56,

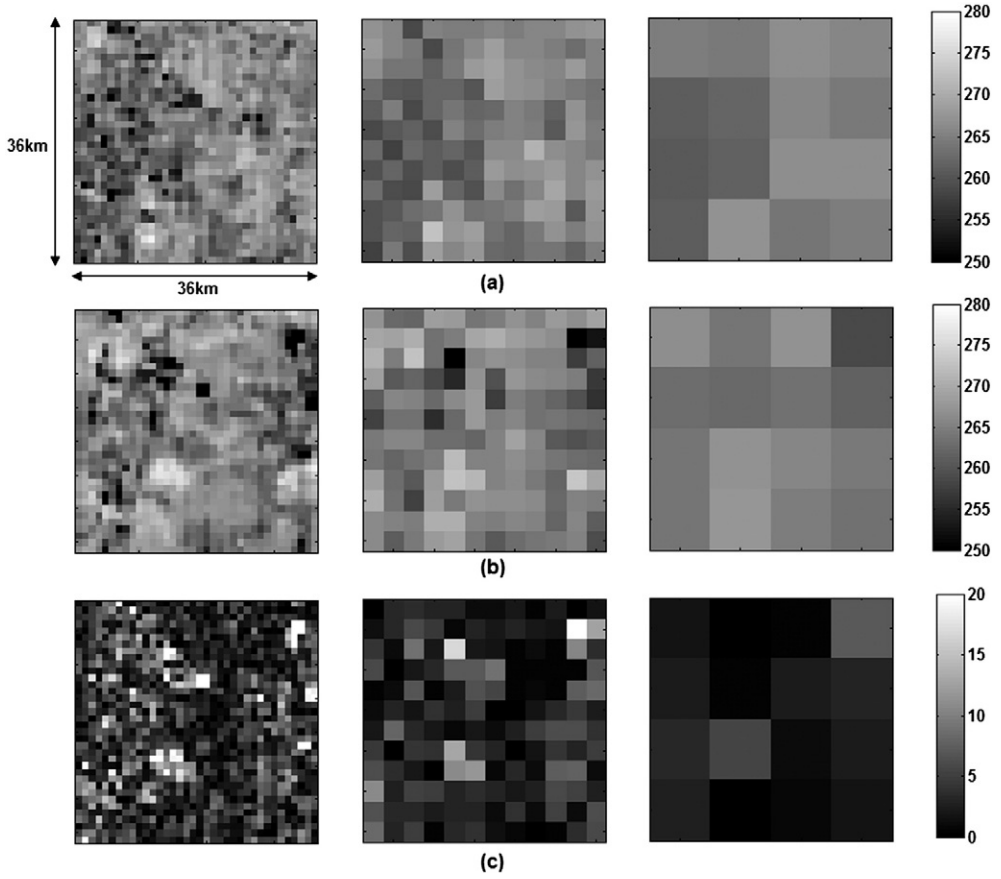

Fig. 7. An example of downscaling results on SMAPEx-3 Day 9 (23rd Sept., 2011): (a) Downscaled brightness temperature (*Tb*) at *v*-polarization for 1 km, 3 km & 9 km resolutions; (b) reference *Tb* at *v*-polarization for 1 km, 3 km & 9 km resolutions; and (c) absolute difference between downscaled *Tb* and reference *Tb* of each 1 km, 3 km & 9 km resolution pixel.

which is approximately 0.15 higher than the average RVI of the entire area, further affecting the correlation between *Tb* and σ in this particular area. The reason is that higher RVI is a consequence of denser vegetation and therefore more influence of the vegetation on the radar observations, and accordingly a higher error when downscaling due to the lower correlation between *Tb* and σ at higher RVI values (see Fig. 3). Therefore, both denser vegetation and more heterogeneous wetness conditions associated to rainfall events have worked together to result in the higher errors on D1 to D4. The influence from the rain event reduced during the dry-down, especially after D4, as shown through the decrease in RMSE from D5 onwards.

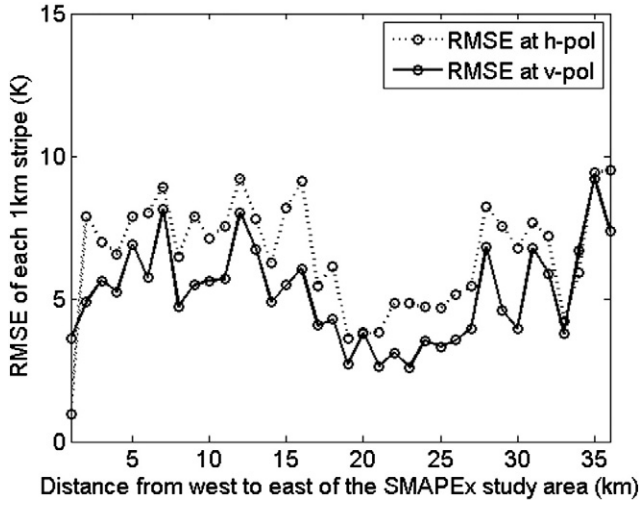

Fig. 8. Downscaling root mean square error (RMSE) at 1 km resolution for each strip, having 36 km length in north–south direction and 1 km width in west–east direction, starting from the west of the SMAPEx study area and progressing to the east, on Day 9 (23rd September, 2011); cropping area in the west, relatively homogeneous grassland area in the middle, and woodland along the river and some forest in the east.

A comparison between this downscaling algorithm and the minimum performance was also conducted. The minimum performance was defined as a uniform *Tb* according to the value of *Tb* at 36 km resolution. In this case, the average RMSE across all 9 days was around 4.8 K at *h*-pol and 4.2 K at *v*-pol at 9 km resolution, being approximately 1.6 K higher than for the baseline downscaling algorithm.

The above analysis on the accuracy of the downscaling algorithm was done after removing the water-bodies and irrigated fields, which collectively represented approximately 1% of the entire SMAPEx study area. The downscaling performance was also evaluated when including the water bodies that had previously been masked out in the aggregation procedure, in order to simulate more realistic SMAP data (as many water bodies will not be reliably identified for masking). Consequently, this allowed the effect of relatively small water bodies on the accuracy of the downscaling approach to be quantified. Without removing the water-bodies, the average RMSE of all nine days at 9 km resolution increased to 3.6 K and 3.4 K at *h*- and *v*-polarizations, respectively, which is approximately 0.7 K higher than results with the water-bodies accurately removed. Therefore, when applying the baseline downscaling algorithm to an area that includes more than 1% of water-bodies the downscaling error would be even larger.

To account for any day-to-day soil temperature variation, β was also estimated using the emissivity and σ, with emissivity calculated as *Tb* divided by soil temperature on that day. The new estimate of β was then multiplied by the soil temperature, before substituting for the previous value of β based on *Tb* and σ. However, the average RMSE of downscaling *Tb* based on this new estimation of β was 3.4 K at *h*-pol

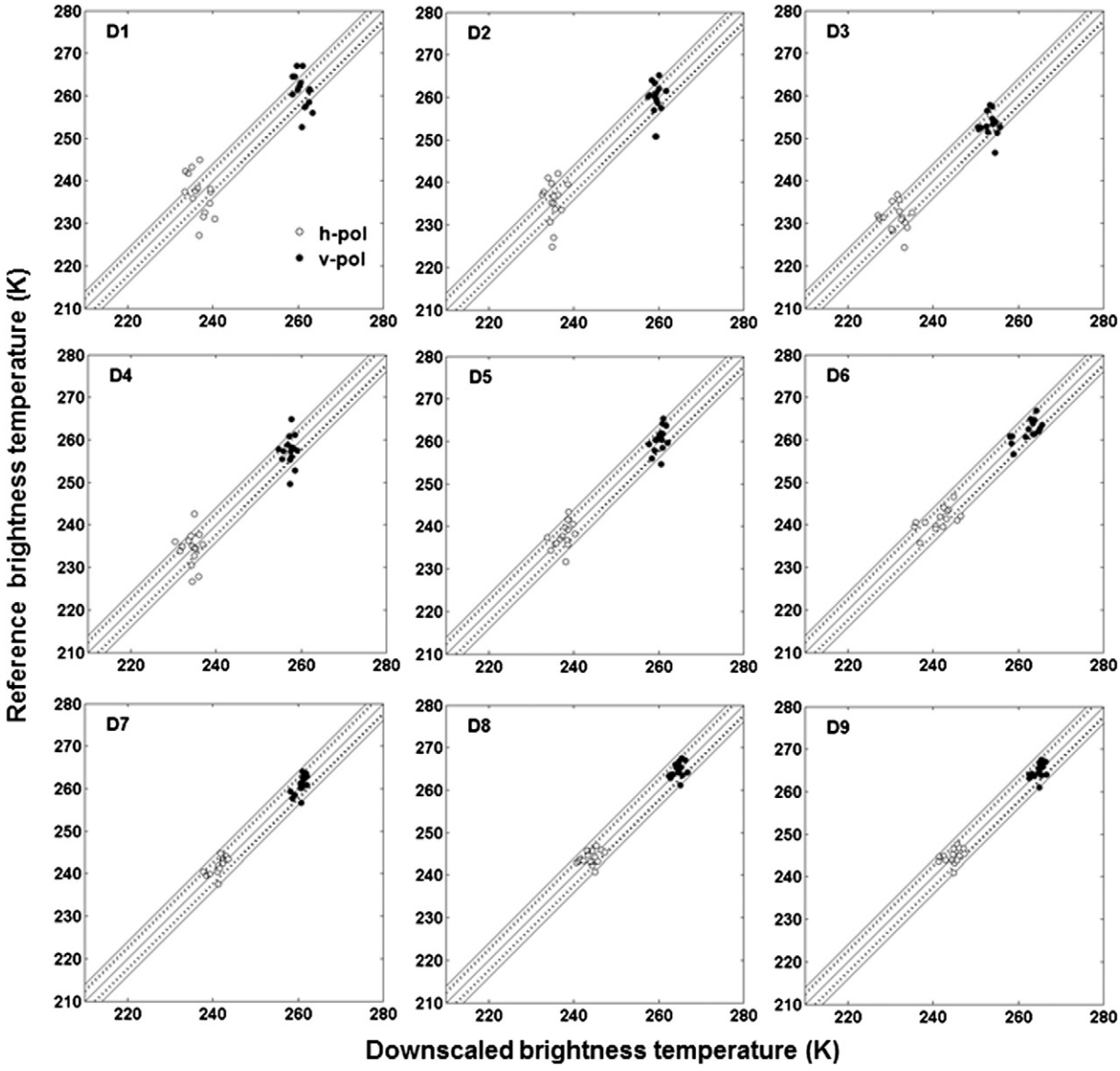

Fig. 9. Scatter plots of downscaled and reference brightness temperature (*Tb*) at 9 km resolution on each of SMAPEx-3 Day 1 to Day 9, at *h*-pol (open dots) and *v*-pol (solid dots); inner black solid line: RMSE is 0 K; two black dashed lines: RMSE = 2.4 K (SMAP *Tb* target accuracy); outer two black solid lines: RMSE = 4 K (SMOS *Tb* target accuracy).

and 2.7 K at *v*-pol at 9 km resolution, being only slightly different to previous results.

4.4. Reliability of baseline downscaling algorithm

In this study, the accuracy of downscaling results was primarily determined by the parameter β as shown in Eq. (1). The main limitation of the downscaling method introduced in Das et al. (2014) is the assumption of a constant β across the entire study area. The parameter β, used to denote the sensitivity of *Tb* to σ, in reality varies with respect to the land surface conditions, as shown in Figs. 4 and 5. Therefore, the assumption of a constant value of β could not represent the real distribution of β due to the heterogeneity of the study area. For example, if the study area was entirely covered by homogenous grassland, then the use of a single β would be more appropriate for use in downscaling. However, as shown in the above results, the variation on land cover types across the entire site, or soil moisture heterogeneity due to raining events in some particular areas, or some water-bodies, or surface roughness, or vegetation evolution due to different seasons would result in different values of β across the site.

As β was estimated from time-series of *Tb* and σ at 36 km, more accurate regression could be obtained from a longer time period so as to make it statistically significant. However, the vegetation and roughness conditions are changing as time goes on, which will result in different β estimates through time. Therefore, a moving window of β estimation should be adopted when applying the downscaling algorithm to a long time period. This is not done in this study but should be acknowledged for future application.

5. Conclusions

The objective of this study was to test the robustness of the baseline downscaling approach proposed for the SMAP mission, using a simulated SMAP data stream from the SMAPEx field campaign in Australia. The errors associated with the downscaling algorithm were assessed for several resolutions of the final downscaled product and at both *h*- and *v*-polarizations. The average RMSE of downscaled *Tb* across 9 days at 9 km resolution was 3.1 K and 2.6 K at *h*- and *v*-polarizations, which increased to 5.5 K and 4.5 K at 3 km resolution, and 8.2 K and 6.6 K at 1 km resolution. The algorithm was found to perform poorly in the early days

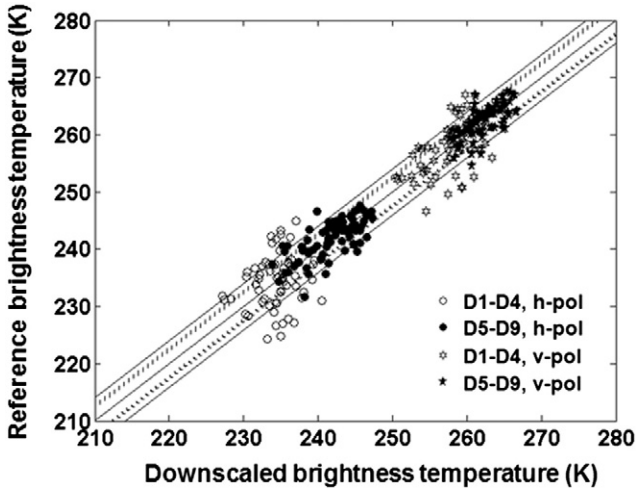

Fig. 10. Scatter plots of downscaled and reference brightness temperature (*Tb*) at 9 km resolution for all SMAPEx-3 acquisitions (Day 1 to Day 9), at *h*-pol and *v*-pol. Solid dots and stars represent data from SMAPEx-3 Day 5 to Day 9, while the open dots and stars represent data from SMAPEx-3 Day 1 to Day 4. Inner black solid line: RMSE is 0 K; two black dashed lines: RMSE = 2.4 K (SMAP *Tb* target accuracy); outer black solid lines: RMSE = 4 K (SMOS *Tb* target accuracy).

of the experiment due to large rainfall events in the study area that created a large spatial heterogeneity in terms of soil moisture content. In contrast, the last 5 days of the experiment, characterized by a drying down period and no rainfall, showed an increase in the algorithm performance, with an RMSE consistently better than 2.4 K at 9 km resolution, indicating that the baseline downscaling algorithm has the potential to fulfill the requirements of SMAP.

It was also shown that the accuracy of the downscaling approach was primarily determined by the correlation between *Tb* and σ, which was in fact affected by the vegetation characteristics across the entire study area and the sensitivity of brightness temperature relative to radar backscatter (as quantified by the slope β of the linear regression). Moreover, it was found that σ at *vv*-polarization was best correlated to *Tb* at both polarizations, therefore being more suitable for use in the downscaling algorithm than σ at *hh*- and *hv*-polarizations. While a better estimation of β at 36 km scale may be expected from SMAP than that achieved here, due to the relatively short nature of this experiment, the impact from temporal changes would be an important consideration.

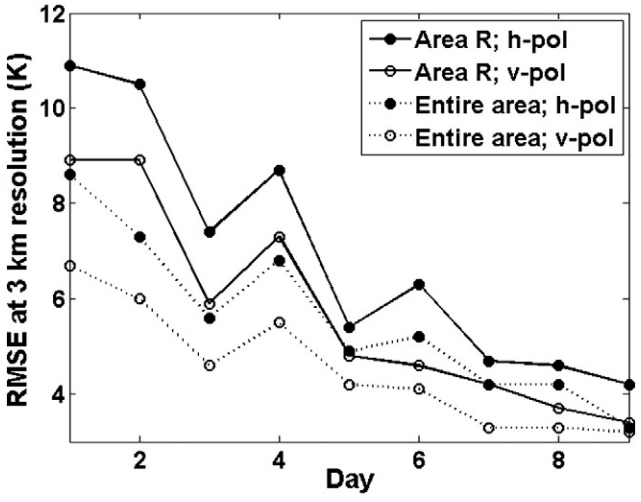

Fig. 11. Comparison between the root mean square error (RMSE) of the north-eastern (area "*R*") of the SMAPEx study area, and RMSE of the entire study area. Calculations are for 3 km resolution at both polarizations across 9 days.

Some preliminary results on the relationship between β and RVI, and the relationship between Γ and RVI have been discussed in this study. They indicate that an improvement in the parameterization of β and Γ may be obtained through their correlation with RVI, allowing a better retrieval and more accurate spatial distribution of β and Γ across the entire area. In future studies it is also important to investigate the estimation of β and Γ at the pixel resolution with respect to land cover, vegetation water content, surface roughness etc., and how these can improve the accuracy of the downscaling algorithm by incorporating this fine scale information into the downscaling approach.

Acknowledgments

The SMAPEx field campaigns and related research development have been funded by the Australian Research Council Discovery (DP0984586) and Infrastructure (LE0453434 and LE0882509) grants. The authors acknowledge the collaboration of a large number of scientists from throughout Australia and around the world, and in particular key personnel from the SMAP team which provided significant contributions to the campaign's design and execution. The authors also acknowledge the scholarships awarded by Monash University to support Xiaoling Wu's PhD research.

References

Albergel, C., Calvet, J. C., Mahfouf, J. F., Rüdiger, C., Barbu, A. L., Lafont, S., et al. (2010). Monitoring of water and carbon fluxes using a land data assimilation system: A case study for southwestern France. *Hydrology and Earth System Sciences*, *14*, 1109–1124.

Albertson, J.D., & Parlange, M. B. (1999). Natural integration of scalar fluxes from complex terrain. *Advances in Water Resources*, *23*, 239–252.

Das, N. N., Entekhabi, D., & Njoku, E. G. (2011). An algorithm for merging SMAP radiometer and radar data for high-resolution soil-moisture retrieval. *IEEE Transactions on Geoscience and Remote Sensing*, *49*, 1504–1512.

Das, N. N., Entekhabi, D., Njoku, E. G., Shi, J. J. C., Johnson, J. T., & Colliander, A. (2014). Tests of the SMAP combined radar and radiometer algorithm using airborne field campaign observations and simulated data. *IEEE Transactions on Geoscience and Remote Sensing*, *52*, 2018–2028.

Draper, C. S., Mahfouf, J. F., & Walker, J. P. (2011). Root zone soil moisture from the assimilation of screen-level variables and remotely sensed soil moisture. *Journal of Geophysical Research, [Atmospheres]*, *116*, D02127.

Entekhabi, D., Das, N. N., Njoku, E. G., Johnson, J., & Shi, J. C. (2012). Algorithm theoretical basis document: L2 & L3 radar/radiometer soil moisture (active/passive) data products. *Initial Release, v. 1*.

Entekhabi, D., Njoku, E. G., O'Neill, P. E., Kellogg, K. H., Crow, W. T., Edelstein, W. N., et al. (2010). The Soil Moisture Active Passive (SMAP) mission. *Proceedings of the IEEE*, *98*, 704–716.

Hain, C. R., Crow, W. T., Mecikalski, J. R., Anderson, M. C., & Holmes, T. (2011). An intercomparison of available soil moisture estimates from thermal infrared and passive microwave remote sensing and land surface modeling. *Journal of Geophysical Research*, *116*, D15107.

Houser, P. R., De Lannoy, G., & Walker, J. P. (2012). *Hydrologic data assimilation.* InTech.

Jackson, T. J., Hsu, A. Y., & O'Neill, P. E. (2002). Surface soil moisture retrieval and mapping using high-frequency microwave satellite observations in the southern great plains. *Journal of Hydrometeorology*, *3*, 688–699.

Kerr, Y. (2007). Soil moisture from space: Where are we? *Hydrogeology Journal*, *15*, 117–120.

Kerr, Y. H., Waldteufel, P., Wigneron, J. P., Martinuzzi, J., Font, J., & Berger, M. (2001). Soil moisture retrieval from space: the Soil Moisture and Ocean Salinity (SMOS) mission. *IEEE Transactions on Geoscience and Remote Sensing*, *39*, 1729–1735.

Kim, Y., & van Zyl, J. (2009). A time-series approach to estimate soil moisture using polarimetric radar data. *IEEE Trans. Geosci. Remote Sens.*, *47*, 2519–2527.

Narayan, U., Lakshmi, V., & Jackson, T. J. (2006). High-resolution change estimation of soil moisture using L-band radiometer and radar observations made during the SMEX02 experiments. *IEEE Transactions on Geoscience and Remote Sensing*, *44*, 1545–1554.

Panciera, R., Walker, J. P., Jackson, T. J., Gray, D. A., Tanase, M.A., Dongryeol, R., et al. (2014). The Soil Moisture Active Passive Experiments (SMAPEx): Toward soil moisture retrieval from the SMAP mission. *IEEE Transactions on Geoscience and Remote Sensing*, *52*, 490–507.

Piles, M., Entekhabi, D., & Camps, A. (2009). A change detection algorithm for retrieving high-resolution soil moisture from SMAP radar and radiometer observations. *IEEE Transactions on Geoscience and Remote Sensing*, *47*, 4125–4131.

Reichle, R. H., Walker, J. P., Koster, R. D., & Houser, P. R. (2002). Extended versus ensemble Kalman filtering for land data assimilation. *Journal of Hydrometeorology*, *3*, 728–740.

Seneviratne, S. I., Corti, T., Davin, E. L., Hirschi, M., Jaeger, E. B., Lehner, I., et al. (2010). Investigating soil moisture–climate interactions in a changing climate: A review. *Earth-Science Reviews*, *99*, 125–161.

Wagner, W., Blsch, G., Pampaloni, P., Valvet, J., Bizarri, B., Wigneron, J., et al. (2007). Operational readiness of microwave remote sensing of soil moisture for hydrologic applications. *Nordic Hydrology*, *38*, 1–20.

Wagner, W., Scipal, K., Pathe, C., Gerten, D., Lucht, W., & Rudolf, B. (2003). Evaluation of the agreement between the first global remotely sensed soil moisture data with model and precipitation data. *Journal of Geophysical Research, [Atmospheres]*, *108*, 4611.

Weaver, C. P., & Avissar, R. (2001). Atmospheric disturbances caused by human modification of the landscape. *Bulletin of the American Meteorological Society*, *82*, 269–281.

Wu, X., Walker, J. P., Rüdiger, C., Panciera, R., & Gray, D. (2014). Simulation of the SMAP data stream from SMAPEx field campaigns in Australia. *IEEE Transactions on Geoscience and Remote Sensing*, *53*, 1921–1934.

Zhan, X., Houser, P. R., Walker, J. P., & Crow, W. T. (2006). A method for retrieving high-resolution surface soil moisture from hydros L-band radiometer and radar observation. *IEEE Transactions on Geoscience and Remote Sensing*, *44*, 1534–1544.